Duffy Antigen Receptor for Chemokines (DARC) Nanodisc-Based Biosensor for Detection of Staphylococcal Bicomponent Pore-Forming Leukocidins

So-Ong Kim, Inkyoung Park, Thierry Vernet, Christophe Moreau, Seunghun Hong, Tai Hyun Park

Duffy antigen receptor for chemokines (DARC) nanodisc-based biosensor for the detection of staphylococcal bicomponent pore-forming leukocidins

So-ong Kim[a, †], Inkyoung Park[b, †], Thierry Vernet[c], Christophe Moreau[c], Seunghun Hong[b*] and Tai Hyun Park[a,d]**

[a] School of Chemical and Biological Engineering, Institute of Chemical Processes, Seoul National ffUniversity, Seoul 08826, Republic of Korea

[b] Department of Physics and Astronomy, and the Institute of Applied Physics, Seoul National University, Seoul 08826, Republic of Korea

[c] Univ. Grenoble Alpes, CNRS, CEA, IBS, F-38000 Grenoble, France

[d] Department of Nutritional Science and Food Management, Ewha Womans University, Seoul 03760, Republic of Korea

[†]These authors contributed equally to this work.

[*] Corresponding author at: Department of Physics and Astronomy, and the Institute of Applied Physics, Seoul National University, Seoul 08826, Republic of Korea.

[**] Corresponding author at: Department of Nutritional Science and Food Management, Ewha Womans University, Seoul 03760, Republic of Korea.

E-mail address: seunghun@snu.ac.kr (S. Hong), thpark@ewha.ac.kr (T. H. Park)

Abstract

Staphylococcus aureus (*S. aureus*) is an opportunistic infectious pathogen, which leads to a high mortality rate during bloodstream infections. The early detection of virulent strains in patient blood samples is of medical interest for rapid diagnosis. One of the main virulent factors identified in patien isolates is the leukocidin gamma hemolysin (HlgAB). HlgAB is a bicomponent pore-forming toxin that binds to specific membrane receptors, such as the Duffy antigen receptor for chemokines (DARC), to lyse immune cells and erythrocytes. Current methods are based on ELSIA or bacterial culture with takes hours to days. For detecting HlgAB with faster response and hishger sensitivity, we developed a biosensor that combines single-walled carbon nanotube field effect transistors with immobilized DARC receptors as biosesing elements. DARC was purified from a bacterial expression system and successfully reconstituted into nanodiscs that preserve binding capability for HlgAB. Dynamic light scattering (DLS) and scanning electron microscopy (SEM) showed an increase of the DARC-containing nanodiscs size in presence of HlgAB, indicating the formation of HlgAB pre-pore or pore complexes. We demonstrate that this sensor could specifically detect the leukocidins HlgA and HlgAB in buffer from a concentration of 1 fM and in a quantitative manner with a LOD of 0.122 fM and a LOQ of 0.441 fM within the dynamic range of 1 fM to 100 pM. The sensor was challenged with human serum spiked with HlgAB as simulated clinical samples, and after dilution for decreasing nonspecific binding, it selectively detected the toxin with similar method detection level (MDL) and apparent dissociation constant as in buffer. This biosensor was demonstrated with remarkable sensitivity to detect HlgAB rapidly holding potential as a tool for fundamental research and clinical applications.

Keywords: leukocidin, gamma-hemolysin, Duffy antigen receptor for chemokines, nanodisc, swCNT-FET

1. Introduction

S. aureus is a common commensal bacterium that can asymptotically colonize human skin, nose and intesine. [1] However, in some case, it becomes an opportunistic pathogen responsible for diverse infections frequently observed worldwide in food poisoning and more critically in hospitals where multiresistant *S. aureus* strains to antibiotics cause severe reduction in therapeutic efficacy. [2-4] The severity of infection ranges widely from mild skin or soft tissue infections to more severe bacteremia, sepsis, infective endocarditis, osteomyelitis, and pneumonia. [5] Especially, mortality rate associated with *S. aureus* bacteremia within 30 days stands at approximately 20%, a statistic that has remained constant since the 1990s. [6, 7] Therefore, an invasive infection of *S. aureus* via blood stream clearly leads to serious clinical consequences if prevention or treatment is not initiated in early phases.

S. aureus is able to secrete numerous virulence factors, including toxins, immune evasion factors, and a plethora of protenaous or non-proteneous factors factors that can facilitate host colonization during infections. [8] Leukocidins from *S. aureus* are secreted as soluble proteins that can specifically lyse leukocytes, thus weakening host defenses. One strain of *S. aureus* related to human infections is capable of producing some cognate pairs of leukocidins: the gamma-hemolysins HlgAB, the leukotoxins LukAB (also known as LukGH), LukED and the Panton-Valentine leukotoxins LukSF-PV. [8] Each bicomponent toxin targets specific innate and adaptive immune cells through specific interactions with membrane receptors and causes death of these specific cells. Among them, gamma-hemolysin HlgAB is secreted by 99% of *S. aureus* isolates, representing a conserved set of leukocidins present in the core genome of *S. aureus*. [8] HlgAB not only targets on leukocytes, but also erythrocytes, providing heme molecules as an iron source and leading to growth of bacteria in host blood. [9] HlgAB also increases vascular

permeability in blood vessels, resulting in vascular injury and fluid extravasation into tissue. [10] Toxicity of HlgAB is determined by their binding capability on several chemokine receptors (such as CCR2, CXCR1, and CXCR2) and DARC present on surfaces of leukocyte, erythrocytes and endothelial cells. [11, 12] HlgAB undergoes oligomerization and assemble into a heterooctameric pore within the plasma membrane of targeted chemokine receptors, which causes osmotic dysregulation and leakage of ions and essential nutrients, leading to cell death. [13-15] Therefore, HlgAB in a patient blood is a critical biomarker for the most frequent infections by *S. aureus* strains and rapid, sensitive and specific biosensing techniques to HlgAB are required for implementing early and appropriate treatments in hospitals and communities.

Rapid detection of *S. aureus* blood samples can be performed by real-time PCR and other more recent techniques such as T2Dx and Hybrisep, which does not require blood culture. [16] T2Dx method is based on magnetic resonance, while Hybrisep uses in situ hybridization methods. Both technology provide responses in hours. More specific detection of leukocidins in blood samples is rarer and it is generally based on enzyme-linked immunosorbent assay (ELISA). [17] However, this method alsorequires several hours in biomedical laboratories. In addition, it is susceptible to interference by staphylococcal protein A which can lead to false-positive results in immunoassays based on mammalian immunoglobiulin G (IgG). [18] Thus, development of biosensors has gained enormous attention for detecting pathogens, toxins, biomarkers and bioactive molecules. [19-26] Especially, electronic devices with biological elements for detecting virulent factors from *S. aureus* in various samples have gained attention thanks to their real-time measurements and simple operation with high sensitivity and selectivity. [27-31] However, none of them could detect or identify leukocidins or use specific membrane receptors as immobilized baits.

94 The utilization of membrane receptors such as DARC in biosensors is challenging since they
95 belong to G-protein coupled receptor (GPCR) family. This family is notoriously known to have
96 a propensity to aggregate when overexpressed in *Escherichia coli* (*E. coli*). [32, 33] Nanodiscs
97 have been utilized for the appropriate structures for GPCR reconstitution due to their membrane
98 mimetic and enhanced stability. [34, 35] Nanodiscs are composed of lipids and membrane scaffold
99 proteins (MSP) that can tightly hold lipids and membrane proteins together, forming
100 biomimetic patches of membranes. Therefore, nanodiscs can provide a native and stable lipid
101 membrane structures for GPCR functions in a variety of environments. [36, 37]
102 Herein, we report the development of a bioelectronic sensor of HlgAB using immobilized
103 DARC in nanodiscs. DARC was overexpressed in *E. coli*, embedded into nanodiscs, and
104 immobilized on single-walled carbon nanotube field effect transistors (swCNT-FETs). This
105 sensor device could detect the binding of HlgA and HlgAB with high sensitivity in real-time.
106 This sensor responded to HlgAB with higher signal amplitude, showing that it could detect the
107 complexes of HlgAB. This sensor also detected HlgAB in spiked human serum as a clinical
108 sample with a sensitivity comparable to that observed in a buffer solution. This sensor is
109 promising for studying interactions between membrane proteins and gamma-hemolysins and
110 developing highly sensitive *in vitro* diagnostic systems of HlgAB.
111
112

2. Materials and Methods

2.1 Protein constructs

For production of gamma-hemolysins in *E. coli*, the genes of *S. aureus* HlgA (UniprotKB-P0A074), HlgB (UniprotKB-P0A077) and HlgC (UniprotKB-Q07227) were synthesized and subcloned into pQE-30 vectors. For expression of DARC in mammalian cells, the full-length of gene of human DARC isoform-2 (UnioprotKB-Q16570) was synthesized and subcloned into modified pXOOM vectors. For production of DARC in *E. coli*, human DARC genes in pXOOM vectors were amplified and subcloned into pET-DEST42 vectors. For production of the membrane scaffold proteins MSP1E3D1 in *E. coli*, the expression vectors for MSP1E3D1 were purchased from Addgene.

2.2 Expression and purification of leukocidins

M15 *E. coli* strains (Qiagen, Germany) were transformed with the expression plasmids including HlgA or HlgB. These transformed strains were cultured in 2 L of Luria-Bertani broth (LB) supplemented with 100 µg/ml ampicillin and 30 µg/ml kanamycin at 37°C under 150 rpm agitation until reaching an optical density (OD) of 0.3. Prior to induction, the culture was pre-cooled at 15°C for 30 minutes under 150 RPM agitation at 15°C. Isopropyl β-D-1-thiogalactopyranoside (IPTG) was then added to a final concentration of 0.5 mM and the cultures were grown overnight. The induced cultures were centrifuged at 4500 g for 15 minutes and the resulting pellet was resuspended in 40 ml of lysis buffer (20 mM HEPES (pH 7.5), 150 mM NaCl, 50 mM imidazole, 1 tablet of cOmplete EDTA-free protease inhibitor (Roche), 10 µg/ml DNase I, and 10 µg/ml RNase). The cells were lysed by subjecting them to four cycles using the microfluidizer LM20 (Microfluidics, USA) at 17000 psi while maintaining a

temperature of 4°C. Subsequently, the lysate was clarified by centrifugation at 38500 g or relative centrifugal force (RCF) for 20 minutes at 4°C. His-tagged proteins were purified using immobilized metal chelate affinity chromatography on a 1 ml His-Trap HP column (Cytiva). Prior to loading the lysate, the column was equilibrated with 20 mM HEPES (pH 7.5), 150 mM NaCl, and 50 mM imidazole. A stepwise elution was performed using elution buffers (20 mM HEPES (pH 7.5), 150 mM NaCl, and 250 mM or 300 mM imidazole). Following purification, the eluate from the final elution step was dialyzed against the buffer containing 20 mM HEPES (pH 7.5) and 150 mM NaCl overnight at 4°C using a Spectra/Por 4 dialysis membrane.

2.3 Cell viability assay with recombinant leukocidins

Human embryonic kidney-293T (HEK-293T) cells were purchased from American Type Culture Collection (ATCC). These cells were cultured at 37°C with 5% CO_2 condition in Dulbecco's Modified Eagle Medium (DMEM) with high glucose (Biowest, USA) supplemented with 10% fetal bovine serum (FBS) and 100 µg/mL of penicillin-streptomycin mix (Sigma-Aldrich, USA). HEK-293T cells were seeded into 96-well plates at a density of 2×10^4 cells/well for 24 h. After that, HEK-293T cells were transfected with 0.1 µg/well of DARC-encoding plasmid using Lipofectamine 3000 (Thermo Fisher Scientific, USA) and incubated overnight. The expression of DARC was verified by western blot analysis using rabbit anti-DARC antibody (Santacruz, USA). For western blot analysis, membrane fraction of HEK-293 cells was quantified with Pierce BCA Protein Assay Kit (Thermo Fisher Scientific, USA) and each sample were loaded with 20 µg per each lane. The cells were then exposed either to HlgA alone or to a mixture of HlgA and HlgB together with 100 nM concentration for each at 37°C for 30 min. For concentration-effect experiments, concentrations were applied sequentially from 3 nM to 1000 nM. Cell viability was measured with Cell Counting Kit-8

(CCK-8) (Dojindo Laboratories, Japan). A volume of 10 µL of CCK-8 reagent was added into each well. Plates were then incubated at 37°C for 2 h. Absorbance at 450 nm was measured using a Spark™ 10M multimode microplate reader (Tecan, Switzerland).

2.4 Cell permeability assay with recombinant leukocidins

For DAPI staining, HEK-293T cells were seeded into 6-well plates at a cell density of 6×10^5 cells/well, cultured for 24 h, and then transfected with 2.5 µg/well of DARC-encoding plasmid using Lipofectamine 3000 (Thermo Fisher Scientific, USA). After incubation at 37°C overnight, recombinant leukocidins HlgA and HlgB were added at a concentration of 100 nM or 1000 nM to the transfected cells in each well and incubated at 37°C for 30 min. Pore formation caused by leukocidins was detected by intracellular staining of DNA with 4',6-diamidino-2-phenylindole (DAPI) at a final concentration 0.1 µg/mL without any fixation. Positive controls for pore formation were treated with 0.1% Triton X-100 instead of the leukocidins. Images of DAPI-stained cells indicating a permeabilized plasma membrane were acquired using a TE300 microscope (Nikon, Japan) with DAPI filter. DAPI-stained cells were counted using the National Institutes of Health (NIH) ImageJ software. For Ca^{2+} influx assay, HEK-293T cells were plated into 96-well plates at 2×10^4 cells/well, incubated for 24 h, and were transfected with 0.1 µg/well of DARC-encoding plasmid using Lipofectamine 3000 (Thermo Fisher Scientific, USA). After incubation overnight, the medium was replaced with Ringer's solution (10 mM HEPES, 5 mM glucose, 140 mM NaCl, 1 mM $MgCl_2$, 1.8 mM $CaCl_2$ and 5 mM KCl, pH 7.4) containing 10 mM Fura 2-acetoxymethyl ester (Fura 2-AM) dye (Thermo Fisher Scientific, USA) for 1 h at 37°C. The cells were then washed with Ringer's solution without the dye and incubated at 37°C for 30 min to cleave intracellular AM esters completely. The fluorescence signal upon addition of recombinant leukocidins HlgA and HlgB

mix was measured at dual excitation at 340 and 380 nm using a Spark™ 10M multimode microplate reader (Tecan, Switzerland).

2.5 Preparation of DARC-containing nanodiscs

The DARC-containing nanodiscs were prepared as previously described. [22] Briefly, the plasmid containing the DARC-encoding sequence was incorporated in *E. coli* and synthesized by the bacterial protein expression system in a form of inclusion body. The proteins were solubilized, dialyzed and then purified by immobilized metal chelate affinity chromatography using HisTrap HP column (Cytiva). Following purification, DARC-containing nanodiscs were reconstituted using purified DARC, membrane scaffold proteins MSP1E3D1 and 1,2-dimyristoyl-sn-glycero-3-phosphocholine (DMPC (, Avanti Polar Lipids, USA) with the molar ratio 1:10:800. The nanodiscs were applied to a size exclusion chromatography (SEC) column Superdex 200 Increase 10/300 GL (Cytiva) to remove unassembled proteins. The concentration of purified nanodiscs was calculated by absorbance value at 280 nm and the Beer-Lambert equation as follows: $A = \varepsilon cL$, where A, ε, c and L were absorbance, molar extinction coefficient, protein concentration and path length, respectively. The molar extinction coefficient of the entire complex at 280 nm absorbance was estimated from the amino acid sequence as follows: $\varepsilon_{nanodisc}$ (121810 M^{-1} cm^{-1}) = ε_{DARC} (67950 M^{-1} cm^{-1}) + 2×$\varepsilon_{MSP1E3D1}$ (26930 M^{-1} cm^{-1}). For identification of DARC-containing nanodiscs, sodium dodecyl sulfate-polyacrylamide gel electrophoresis (SDS-PAGE) and Western blot analysis were performed. Nanodisc samples were migrated on a polyacrylamide gel, which was then stained with Coomassie Blue solution (Coomassie Blue 0.5 g/L, acetic acid 7% (v/v), methanol 40% (v/v)) for 1 h at 25°C and destained in acetic acid 7% (v/v) and methanol 5% (v/v)) overnight at 25°C. Western blot was then performed using rabbit anti-DARC antibody (Santacruz, USA) and mouse anti-His tag

antibody (Santacruz, USA) as primary antibody at 1:1000 dilution. Goat anti-rabbit IgG-horseradish peroxidase (HRP) antibody and goat anti-mouse IgG-HRP antibody were used as secondary antibody at 1:5000 dilution.

2.6 Size analysis of DARC-containing nanodiscs

The size of purified DARC-containing nanodiscs was analyzed by a DLS spectrophotometer DLS-7000 (Otsuka Electronics, Japan) under the following measurement conditions: temperature (25°C), refractive index (1.3315), and viscosity (0.891). A disposable, small volume cuvette (Malvern Panalytical, Marvern, UK) was used to measure size distribution. For measurements in the presence of leukocidins, DARC-containing nanodiscs were prepared at a concentration of 1 nM and mixed with bovine serum albumin (BSA) (negative control) or with the combinations of gamma-hemolysins at a final concentration of 1 nM for each added protein. Prepared samples were incubated at 37°C for 30 min. The size of DARC-containing nanodiscs in presence of leukocidins or BSA was analyzed with the same DLS method as mentioned before.

2.7 Fabrication of swCNT-FET

swCNTs were dispersed in 1,2-dichlorobenzene by applying ultrasonication for 4 h to final concentration of 50 µg/mL. For selective adsorption of swCNT assembly, an octadecyltrichlorosilane (OTS) monolayer with hydrophobic terminal groups was patterned on the SiO_2 substrate via photolithography. The patterned substrate with an OTS monolayer was immersed in the swCNT solution for 20 s. Then, swCNTs were selectively adsorbed on polar

SiO_2 region avoiding non-polar OTS monolayer patterns. Excess swCNT suspension was washed out with 1,2-dichlorobenzene. Source and drain electrodes were fabricated on the substrate via photolithography and thermal evaporation. Exposed swCNT channels were 3 μm wide and 170 μm long.

2.8 Functionalization of swCNT-FET with DARC-containing nanodiscs

For immobilization of DARC-containing nanodiscs, 1 mM of 1-pyrenebutanoic acid succinimidyl ester (1-PSE) in methanol was used as a linker. First, 1-PSE was used to treat channel regions followed by incubated at room temperature (RT) for 1 h. Channel regions were rinsed with double distilled water (DDW) three times. The solution of DARC-containing nanodiscs was applied to the same regions followed by incubation at RT for 1 h. All immobilization processes were performed under humidified conditions to prevent evaporation of solutions. Functionalized sensors were rinsed with 0.1× Dulbecco's Phosphate Buffered Saline (dPBS) three times. For verifying the immobilization of DARC-containing nanodiscs on a swCNT-FET, field emission scanning electron microscopy (FE-SEM, Auriga Zeiss, Germany) images were captured. After the devices were completely rinsed with 0.1× dPBS 3 times, DARC-containing nanodiscs were fixed with OsO_4 1% in 0.1× dPBS buffer at RT for 1 h. FET devices were then rinsed using DDW 3 times and dehydrated with sequential 30%, 60%, 90% and 100% ethanol (EtOH) incubation for 10 min each. Samples were freeze-dried overnight and stored at -80°C before SEM analysis. All samples were sputter-coated by Pt at a thickness of 2 ~ 10 nm before SEM images were captured.

2.9 Sample preparations

All tested leukocidins were prepared by diluting samples with 0.1× dPBS (pH 7.4) for the real-time detections of leukocidins. Human serum was purchased from Sigma-Aldrich (USA) to prepare simulated clinical samples. Human serum was thawed at 37°C and centrifuged at 3000 g or RCF for 15 min at 4°C. Supernatants were filtered using a 0.22 μm syringe filter (Sartorius, Germany) and stored at -80°C until used. Prepared human serum was diluted to a concentration of $1/10^3$ with 0.1× dPBS for treating to the sensors with a concentration of $1/10^4$ and spiked with leukocidin HlgAB at various concentrations. For preparations of bacterial supernatants, *S. aureus* ATCC 6358 (Korean Collection for Type Cultures (KCTC), Republic of Korea) and *E. coli* DH5α (Thermo Fisher Scientific, USA) were used. *S. aureus* was streaked from the frozen stock on from a brain heart infusion (BHI) media agar plate and single colony from the BHI plate was inoculated into 50 mL BHI broth media. Cells were incubated in a shaking incubator at 150 rpm at 37 °C overnight. Cells were centrifuged at 3000 g for 5 min and supernatants were harvested and filtered using a 0.22 μm syringe filter. For the control tests, *E. coli* DH5α was used and supernatants of *E. coli* were harvested under the same procedure of supernatants. Each supernatant was diluted with 0.1 × dPBS including $1/10^3$-dilluted human serum for a simulated clinical sample.

2.10 Real-time electrical measurements

For real-time monitoring of leukocidin interactions with DARC on FET devices, leukocidin samples were prepared with 0.1× dPBS for dilutions. Current changes between source and drain electrodes were measured in real time using a Keithley 2636 A source meter (Keithley, USA) and a MST 8000 probe station (MS Tech, South Korea). Voltage between source and drain

electrode was maintained at 0.1 V. A 20 μL droplet of 0.1× dPBS was placed on channel regions and 2 μL of diluted samples was injected sequentially into the droplet of buffer. Dilution factor ranged from 10^{-16} to 10^{-8}.

3. Results and Discussion

3.1 Schematic of a bioelectronic sensor for detecting bicomponent pore-forming toxin HlgAB

Figure 1 shows a schematic diagram depicting the detection of pore-forming activity of HlgAB using a swCNT-FET device functionalized with DARC-containing nanodiscs. Here, swCNT-FET device was fabricated and DARC-containing nanodiscs were immobilized on CNT channel regions with1-PSE as the linker. Leukocidins bound to DARC in nanodiscs. HlgAB is known as a bicomponent pore-forming toxin. Its targeting capability is derived from S component, HlgA. [38,39] Firstly, HlgA targets and binds to DARC. Then HlgB, F component, is assembled with HlgA and forms a pore. HlgAB may form intermediate pre-pore assemblies on the extracellular side of DARC or form pores in DARC-containing nanodiscs. [40] These binding events will lead to changes of net charges in sensing areas. Since HlgAB proteins have positive charges (+23.63) in the buffer at pH 7.4 due to their isoelectric point (pI) values (9.53 for HlgA and 9.18 for HlgB), the conductance of p-type semiconducting CNT channel will decrease after HlgAB binding. [41,42]

3.2 Cell lytic activity of HlgAB depends on DARC expression

To assess cell lytic activity of gamma-hemolysins on DARC-expressing cells, HEK-293T

295 cells were transiently transfected with DARC-encoding plasmid. Western blot with anti-DARC
296 antibody demonstrated the expression of DARC in HEK-293T cells with a band at an expected
297 size of 35.5 kDa (**Figure S1**, red arrow). These cells were then used for *in vitro* assay of cell
298 lytic activity of recombinant leukocidins. **Figure 2a** shows cell viability test for assessing
299 cytotoxicities of various combinations of gamma-hemolysins. Equimolar concentrations of
300 two-component gamma-hemolysins (HlgAB, HlgCB and HlgAC) as well as single gamma-
301 hemolysins were added at 100 nM to DARC-expressing cells. Only HlgAB significantly
302 decreased cell viability. These results confirmed the specific cytotoxicity of HlgAB on cells
303 expressing DARC as previously reported. [12]

304 **Figure 2b** shows concentration-dependent cytotoxicity of HlgAB specifically on cells
305 expressing DARC. The cytotoxic effect on DARC-expressing cells was significant for HlgAB
306 at concentrations equal to or higher than 100 nM compared to mock-transfected cells. Cell
307 viability decreased to ~50% at 100 nM and to ~30% at 1 μM. These results showed that HlgAB
308 were functional and generated a cytotoxic effect specifically on HEK-293T cells expressing
309 DARC as previously reported. [10]

310 In physiological conditions, HlgAB can bind to DARC and form a pore, leading to leakage
311 of small molecules through the plasma membrane. To assess if HlgAB formed pores, DAPI
312 staining and Ca^{2+} influx assay were performed. **Figure 2c** shows DAPI staining images after
313 treating cells with 1000 nM of HlgAB. Statistics are shown in **Figure 2d**. DAPI staining was
314 used as a standard assay for cell permeability based on its membrane impermeability and its
315 ability to stain nucleus of permeabilized cells. Positive controls were performed by
316 permeabilizing cells with 0.1% Triton X-100. While DAPI could not pass through cell
317 membrane in mock-transfected cells regardless of the existence of HlgAB, DAPI significantly
318 passed through the cell membrane of DARC-expressing cells when 1000 nM HlgAB was added

and incubated for 30 min. A second method of assessing cell permeabilization was measuring Ca^{2+} influx with fluorescent Fura-2 AM probe accumulated intracellularly. When cytosolic concentration of Ca^{2+} increased, the fluorescence signal proportionally increased. **Figure 2e** shows a clear increase of the fluorescence when DARC-expressing cells are incubated with 100 nM of HlgAB, indicating a Ca^{2+} influx induced by the toxins. No Ca^{2+} influx was observed for non-transfected-cells, confirming that Ca^{2+} influx induced by HlgAB was DARC-dependent. These results of DAPI staining and Ca^{2+} influx support the ability of HlgAB to permeabilize cells by interacting specifically with DARC to form pores that lead to cell death.

3.3. Characterization of DARC-containing nanodiscs

DARC was cloned into *E. coli* expression vector pET-DEST42 and produced from *E. coli* BL21 strains. It is known that GPCRs overexpressed in *E. coli* are insoluble inclusion bodies in the cytosol. [32, 33] Under our experimental conditions, DARC was also mainly expressed as inclusion bodies. Its solubilization was achieved using harsh detergents such as SDS. The detergents were then removed by dialysis and Bio-Beads. Membrane scaffold protein MSP1E3D1 was also expressed in *E. coli* but in a soluble form. During the reconstitution of DARC into nanodiscs, the molar ratio of DARC, MSP1E3D1, and DMPC was set as 1:10:800 for optimizing the size distribution of nanodiscs under 20 nm. After self-assembled DARC-containing nanodiscs were purified by size exclusion chromatography, they were subjected to SDS-PAGE, Western blot, and DLS analyses for quality control.

Figure 3a shows SDS-PAGE gel loaded with DARC-containing nanodiscs and stained by Coomassie blue. Two bands (red arrows) with molecular weights similar to theoretical molecular weights of 39 kDa and 33 kDa for DARC and MSP1E3D1, respectively, were

observed. Western blot analysis confirmed the nature of these two bands using anti-DARC antibody (**Figure 3b**) and anti-His antibody (**Figure 3c**). These results indicated that DARC was successfully reconstituted into nanodiscs.

Figure 3d shows DLS profile of purified DARC-containing nanodiscs, revealing an average diameter of 15.9 nm. These nanodiscs showed one sharp peak, inferring that purified nanodiscs had a homogeneous size distribution. DLS can be utilized as a tool for characterizing protein aggregation or protein-protein interactions. [43, 44] Therefore, we used DLS to assess the interaction of HlgAB with DARC-containing nanodiscs since the binding event of HlgAB (~35 + ~37 kDa for HlgA and HlgB, respectively) on DARC (~39 kDa)-containing nanodiscs should be detectable. **Figure 3e** shows DLS profiles of nanodiscs treated with various gamma-hemolysins. Bovine serum albumin (BSA, negative control) (1 nM) or various gamma-hemolysin combinations was incubated with DARC-containing nanodiscs and size distributions of samples were then measured by DLS. They are summarized in the legend of **Figure 3e**. DARC-containing nanodiscs alone had a size of 15.9 nm. The average size of BSA or leukocidins alone was 3-5 nm (Data not shown). The average size of DARC-containing nanodiscs treated with BSA and all combinations of leukocidins was between 16.8 nm and 18.9 nm except for HlgAB, which had a ~2.5-fold larger average size (40.2 nm). These results confirmed that HlgAB could specifically bind on DARC-containing nanodiscs and significantly increase the hydrodynamic radius of these nanodiscs. Two hypotheses could explain such size increase: 1) HlgAB could bind to DARC and form pre-pore or pore structures in the lipid bilayer surrounding DARC in nanodiscs. However, the diameter of the nanodiscs was constrained by the length of the surrounding MSP protein, which could hinder insertion of such large pores; 2) HlgAB could bind to DARC and remain attached as a dimer or higher orders of oligomers to the extracellular side of DARC. The increase of the height would also

366 increase the hydrodynamic radius as observed. Thus, it was likely that this size increase of the
367 nanodiscs was mainly due to the formation of large HlgAB complexes on the extracellular side
368 of DARC or potentially due to formation of pore structures by displacement of lipid molecules.
369 The structure of the HlgAB pore (PDB: 3B07) indicates a diameter of 11.4 nm of the complex.[15]
370 The size of the DARC-containing nanodiscs being ~16 nm, the increase of size to ~40 nm in
371 presence of HlgAB suggests that two complexes (pre-pore or pore) are bound to the DARC-
372 nanodiscs: 16 nm (DARC-containing nanodisc) + 2×11.4 nm (HlgAB octameric complex) =
373 38.8 nm. Dimers of DARC have been reported and could explain the potential presence of two
374 HlgAB complexes. [45] While the size of nanodiscs is relatively homogenous and constrained by
375 the length of the surrounding MSP, nanodiscs composed of non-circularized MSP (like
376 MSP1E3D1 used in this study) can fused and form very large nanodiscs (≤ 90 nm) when they
377 are close to each other and additional molecules are inserted in the lipid bilayer. [46] These
378 observations raise the hypothesis that HlgAB binding on DARC could bring together two
379 DARC-containing nanodiscs during the formation of pre-pore complex and that the insertion
380 of pores in the lipid bilayer could induce the fusion of nanodiscs up to a size of 40 nm.
381

382 *3.4. Real-time detection of bicomponent pore-forming toxin HlgAB by swCNT-FET devices*
383 *functionalized with DARC-containing nanodiscs*

384 **Figure 4a** depicts a schematic diagram of two different responses of swCNT-FET devices
385 functionalized with DARC-containing nanodiscs upon introduction of single- or two-
386 component leukocidins. When only single-component HlgA was added, HlgA molecules
387 recognized DARC receptors on the sensor device and bound to the nanodiscs without forming
388 pores or complexes. On the other hand, when two-component HlgA and HlgB were added,

receptor-bounded HlgA molecules could recruit HlgB molecules to form octameric complexes. These different responses resulted in different changes in charge distribution near the sensing area. Since HlgA and HlgB proteins have positive net charges as discussed in **Figure 1**, two-component HlgAB could form complexes or pore structures and induce more accumulation of positive charges than single-component HlgA, leading to different signal amplitudes of the sensor device.

Figure 4b shows field-emission scanning electron microscopy (FE-SEM) images of DARC-containing nanodiscs immobilized on the channel region before and after HlgAB binding. The FE-SEM samples were prepared with paraformaldehyde and osmium tetroxide solution for fixation of protein and lipids in the nanodiscs, respectively. The surface of nanodisc-immobilized swCNT-FET device was coated with a 3 nm Pt layer for a high electron scattering rate. The images showed attachment of nanodiscs onto CNT network lines clearly. The average diameter of DARC-containing nanodiscs was estimated as 20 nm before HlgAB binding. After HlgAB binding, diameters of DARC-containing nanodiscs were increased about 40 nm up to 80 nm (right image in **Figure 4b**), consistent with the broader size distribution of DARC-containing nanodiscs after HlgAB binding estimated by DLS measurement as shown in **Figure 3e**. Also, these results indicated that these swCNT-FET devices were successfully functionalized with DARC-containing nanodiscs. Size increase of DARC-containing nanodiscs based on complex formation of HlgAB also occurred after immobilizing these nanodiscs on the channel region of the devices. On the other hands, **Figure S2** shows FE-SEM image of a pore structure of HlgAB bound to DARC-containing nanodiscs on swCNT-FET. This result demonstrates that HlgAB bound to DARC formed not only a pre-pore complex but pore structure, indicating this device could have a potential to measure a pore-forming activity of HlgAB to DARC.

Figure 4c shows the real-time monitoring on a swCNT-FET device functionalized with DARC-containing nanodiscs to HlgAB solutions. Decrease of source-drain currents were observed as HlgAB concentrations increase. The current change was detected at first when treated with 1 fM of HlgAB in this experiment. Limit of detection (LOD) was calculated as the concentration that corresponds to the signal-to-noise (S/N) ratio of 3. The LOD of the device for HlgAB was 0.122 fM. [47] Limit of quantitation (LOQ) was calculated as the concentration that corresponds to the S/N ratio of 10, and the LOQ of the device for HlgAB was 0.441 fM. [48] In this buffer (0.1×dPBS at pH 7.4), HlgAB had a net positive charge since their pI was 8.94 (calculated). The swCNT used in this study was a p-type semiconductor. Thus, binding of positively charged HlgAB to DARC could lead to a decrease of source-drain current. Responses were slower than the ones from volatile compounds due to much higher molecular weights of leukocidins (~35 kDa) that could slow down the diffusion speed of molecules after adding toxins into the buffer. [49, 50] A similar response of the swCNT-FET device functionalized with DARC-containing nanodiscs to HlgA solutions was provided in **Figure S3**. Surface plasmon resonance has previously reported the binding of HlgA alone on purified and immobilized DARC. [11] Other gamma-hemolysin HlgB or HlgC alone cannot make any change of currents in **Figure S4**, showing that responses of the sensor require binding to DARC in the nanodiscs.

Next, we used empty nanodiscs composed of DMPC and MSP1E3D1 only for confirming the role of DARC in the biosensor. We functionalized the swCNT-FET with empty nanodiscs under the same conditions and procedures, and treated with HlgAB to the biosensor. Figure S5 shows the real-time monitoring on the swCNT-FET device functionalized with empty nanodiscs to HlgAB. This device also responded to HlgAB, but higher concentration of HlgAB at 10 pM was required to induce current change compared to when functionalized with DARC-

containing nanodiscs. Also, the current change was smaller than the change with DARC-containing nanodiscs. We supposed it was because HlgA could bind to lipid membrane non-specifically, but HlgAB couldn't form a pore structure on the DMPC membrane. [51, 52] Consequently, this result confirmed that DARC is a key element for sensitivity and selectivity to HlgAB in the fabricated sensor.

Figure 4d shows concentration-dependent responses of CNT-FET devices functionalized with DARC-containing nanodiscs to single-component HlgA and two-component HlgAB solutions. Here, detection signals were defined as relative changes of CNT channel conductance with respect to the initial value ($\Delta G/G_0$) at a given leukocidin concentration. Detection signals at a single concentration were repeatedly measured with three devices to acquire average values and standard errors. Our device responded to leukocidin solutions from a concentration of 1 fM. The response was saturated at a concentration of around 100 pM, indicating the dynamic range of our sensor device. Its dose-dependent responses could be fitted by the Hill equation written as $\Delta G/G_0 = C^n/(K_d^n+C^n)$, where C, K_d, and n were the concentration of leukocidin, the dissociation constant for the binding of leukocidins to DARC-containing nanodiscs, and Hill's coefficient, respectively. [53, 54] Calculated dissociation constants of HlgA and HlgAB to DARC-containing nanodiscs were 5.94×10^{-14} M and 6.96×10^{-14} M, respectively. These two values were similar, inferring that binding affinity of HlgAB was similar to that of HlgA in the fabricated sensor platform, which is in agreement with the consensual mechanism of binding of the S component (HlgA) on the receptor, while HlgB is recruited for pore formation. Thus, these similar values of K_d between HlgA and HlgAB suggest that HlgB does not affect the apparent affinity in this sensor, consistent with the role of F component. Importantly, the amplitudes of maximal signal responses to two-component HlgAB (~40%) were more than twice as large as those to single-component HlgA (~20%), which could be

interpreted as a higher density of positive charges of HlgAB in CNT channel region than that of HlgA. This increase of signal amplitude was consistent with the size increase of DARC-containing nanodiscs after HlgAB binding estimated by DLS measurement as shown in **Figure 3d** and **3e**. This size increasing behavior was not observed in the case of HlgA binding. These results showed that our sensor device could be used to detect bicomponent pore-forming HlgAB.

Next, we assessed the biosensor's ability to detect HlgAB in human serum mimicking clinical samples from infected patients. Detecting HlgAB with high sensitivity in blood samples appears to be relevant for diagnosis of bacteremia caused by *S. aureus*. [55, 56] To determine optimal conditions for avoiding false-positive responses, serial dilutions of human serum were applied on bare swCNT-FET and conductance changes were observed for dilutions up to $1/10^3$, but not to $1/10^4$ or higher dilutions (**Figure S6**). **Figure 4e** shows dose-dependent responses of swCNT-FET devices functionalized with DARC-containing nanodiscs to HlgAB diluted in human serum compared to dilutions in buffer. Concentration-dependent responses to HlgAB diluted in human serum were also analyzed by fitting them with the Hill equation. The fitted response curve of human serum case showed almost similar behavior to that of the buffer case. The K_d value of HlgAB in human serum was 3.57×10^{-14} M, similar to the K_d value of HlgAB in buffer solution (6.96×10^{-14} M). Moreover, amplitudes of maximal signal responses to HlgAB in human serum were about 40%, consistent with those in buffer solution. These results showed that human serum did not affect the dose-dependent response of the sensor device to HlgAB, indicating that our sensor device could be used to detect pore-forming toxin HlgAB even in clinical samples from infected patients.

Finally, we used the culture of *S. aureus* to verify the medical applications of the biosensor. *S. aureus* ATCC 6538 was used as a model of *S. aureus* due to its expression of gamma-

hemolysins, while *E. coli* DH5α was used as a negative control[57, 58]. **Figure S7** shows the real-time monitoring on a swCNT-FET device functionalized with DARC-containing nanodiscs to the bacterial supernatants. The current decrease was detected at first when treated with $1/10^7$-diluted *S. aureus* supernatants and the change increased as the higher concentration of *S. aureus* supernatants was treated. While, there was no response to *E. coli* supernatants, which showed selectivity in our sensor devices. The concentrations of gamma-hemolysins in *S. aureus* supernatants were estimated as 1 nM to 100 nM[59, 60]. Thus, the concentration of HlgAB in $1/10^7$ diluted supernatants was expected to be 0.1 fM to 10 fM, which was consistent with a limit of detection (LOD) of 0.122 fM in our devices. These results show that our devices could detect *S. aureus* supernatants in simulated clinical samples, indicating our sensor device could have a potential to be applied in the clinical field.

4. Conclusion

Herein, we developed a biosensor for rapid and sensitive detection of leukocidins HlgAB using swCNT-FETs functionalized with DARC-containing nanodiscs. In the present study, we validated the activity of purified recombinant HlgAB using cell viability and permeability tests with a human cell line HEK-293T transiently transfected with DARC-encoding plasmid. A bioelectronic sensor was then designed for detecting HlgAB using DARC-containing nanodiscs as a bioelement. DARC was successfully expressed in *E. coli*, purified, and reconstitued into nanodiscs of 15.9 nm in size. DLS measurements in the presence of various compositions of single- or two-component gamma-hemolysins interestingly showed a large increase in the average size of DARC-containing nanodiscs only in the presence of HlgAB**.** This result indicated that HlgAB was bound to DARC incorporated in the nanodiscs and formed large complexes or pore structures on DARC. DARC-containing nanodiscs were immobilized on the channel region of the swCNT-FET device with 1-PSE as a linker. This was confirmed by FE-SEM. The fabricated biosensors detected HlgA alone and HlgAB with a LoD of 1 fM and showed concentration-dependent response which was saturated at 100 pM. This biosensor detected HlgA and HlgAB with similar apparent dissociation constants, but with higher signal amplitudes (~2-fold). Thus, this sensor could detect the complex formation of HlgAB in response on DARC-containing nanodisc compared to HlgA alone. Medical applications of this biosensor are envisioned for blood testing of HlgAB contamination due to *S. aureus* strains expressing these virulent factors in the bloodstream. Due to false-positive signals in diluted serum until $1/10^3$, measurements with HlgAB were performed in diluted serum at $1/10^4$. Results confirmed the ability of this DARC-based biosensor to detect HlgAB in diluted human serum with similar apparent K_d and LoD than in buffer.

S. aureus strains can secrete different leukocidins, including LukED or non-cognate pairs of HlgA/LukD or LukE/HlgB that are also able to bind to DARC and form pores. The DARC-based biosensor will detect all of them since the specificity of the binding depends on the S component (HlgA or LukE). Thanks to the multiplex capabilities of on-chip transistors and the specificity of interaction of leukocidins with other receptors (e.g. HlgA on CCR2, LukE on CCR5), it is conceivable to develop biosensors composed of different receptors to identify the leukocidins present in samples. [61]

These biosensors have numerous advantages: 1) rapid response (seconds to min) compared to ELISA (> 1 h); 2) suitable for microelectronics; 3) label-free; 4) high sensitivity (fM) compared to ELISA (10 pM) [62]; 5) high specificity for *S. aureus* leukocidins; 6) stability of the receptor in nanodiscs; 7) multiplexing capacities for *in situ* controls and leukotoxin identification with various receptors; 8) potential for miniaturization; 9) low volume of samples. On the other hand, the disadvantages are: 1) it requires membrane protein purification and reconstitution in nanodiscs, which could be tricky for some receptors. However, the bacterial expression system that is used in this study, is the fastest and the cheapest one, and the amount of functional receptor required for immobilization is low.; 2) it is a single-use test when positive. However, medical *in vitro* diagnostic systems are single-use, and recycling of chips are theoretically possible by replacing the immobilized nanodiscs.; 3) tested blood samples had to be diluted $1/10^4$ due to non-specific binding. However, improvements could be explored with saturation of the non-specific binding surface.

This technology has promising applications in basic research for studying leukocidins binding on membrane receptors and in the clinical field for early detection of gamma-hemolysins in blood samples and diagnosis of virulent toxins from *S. aureus* in the bloodstream.

Associated Contents

Supporting Information

Figure S1: Identification of DARC expression in HEK-293T. Figure S2: SEM image of a pore structure of HlgAB bound to DARC-containing nanodiscs. Figure S3: Real-time responses of the fabricated device to HlgA only. Figure S4: Real-time responses of the fabricated device to HlgC, HlgB and HlgA consecutively. Figure S5: Real-time responses of the device functionalized with empty nanodiscs to HlgAB. Figure S6: Control test of the swCNT-FET to diluted human serum. Figure S7: Real-time responses of the fabricated device to supernatants from *S. aureus* and *E. coli* in simulated clinical samples.

Acknowledgements

We are grateful to Sébastien Granier and Claire Grison for providing DARC cDNA. S. Hong would like to acknowledge the support from the National Research Foundation of Korea (NRF) funded by the Ministry of Science and ICT (MSIT) of Korea (No. RS-2023-00208252) and Samsung Electronics Co. Ltd (No. 201209-07908-01). This study was supported by the Technology Innovation Program (20020801, Construction of international standardization basis for the biodigital biosense) funded by the Ministry of Trade, Industry & Energy (MOTIE), Republic of Korea. IBS acknowledges integration into the Interdisciplinary Research Institute of Grenoble (IRIG, CEA). S. K. and I. P. contributed equally to this paper.

Figure captions

Figure 1. Diagram of the swCNT-FET functionalized with DARC-containing nanodiscs. DARC-containing nanodiscs were immobilized on swCNT with 1-pyrenebutanoic acid succinimidyl ester (1-PSE) as the linker. amma-hemolysin HlgAB binds to DARC and forms pore structures. The fabricated sensor is expected to decrease channel conductance.

Figure 2. Cell viability test and permeability test for leukocidins from *S. aureus*. (a) Cell viability test of HEK293T transiently transfected with DARC followed by treatment with various combinations of leukocidins at 100 nM. (b) Cell viability relying on HlgAB concentrations in cells with or without the expression of DARC. (c) Fluorescence images after DAPI staining and applications of 100 or 1000 nM of HlgAB for cell permeability test. (d) Statistical analysis of cell permeability test results using the relative number of fluorescent cells as permeabilized cells. (e) Statistical analysis of calcium influx assay using Fura-2 AM as an intracellular probe. Results are presented as percentages of intracellular Ca^{2+}-dependent fluorescence induced by 100 nM HlgAB. All data are expressed as mean ± standard deviation ($n = 3$, $*p<0.05$, $**p<0.01$, $***p<0.001$ in the t-test).

Figure 3. Production, reconstitution, and characterization of DARC-containing nanodiscs. (a) SDS-PAGE gel with Coomassie blue staining for DARC-containing nanodiscs. (b) Western blot analysis of DARC-containing nanodiscs with anti-DARC antibody. (c) Western blot analysis of DARC-containing nanodiscs with anti-His tag antibody. (d) Dynamic light scattering profile of purified DARC-containing nanodiscs. (e) Dynamic light scattering profiles

585 of DARC-containing nanodiscs treated with various compositions of gamma-hemolysins.

586

587 **Figure 4.** Detection of leukocidin HlgA and HlgAB using bioelectronics based on swCNT-FET
588 functionalized with DARC-containing nanodiscs. (a) Diagrams of possible responses after
589 treating fabricated bioelectronics with leukocidins. (b) SEM images of immobilized DARC-
590 nanodiscs on swCNT-FET before and after treating with HlgAB. (c) Real-time detection of
591 HlgAB in the sensor with increasing concentrations of HlgAB. (d) Concentration-response
592 curves of HlgA and HlgAB. (e) Concentration-response curves of HlgAB diluted in 0.1×dPBS
593 and human serum. Data are expressed as mean ± standard deviation (n = 3)

Figure 1.

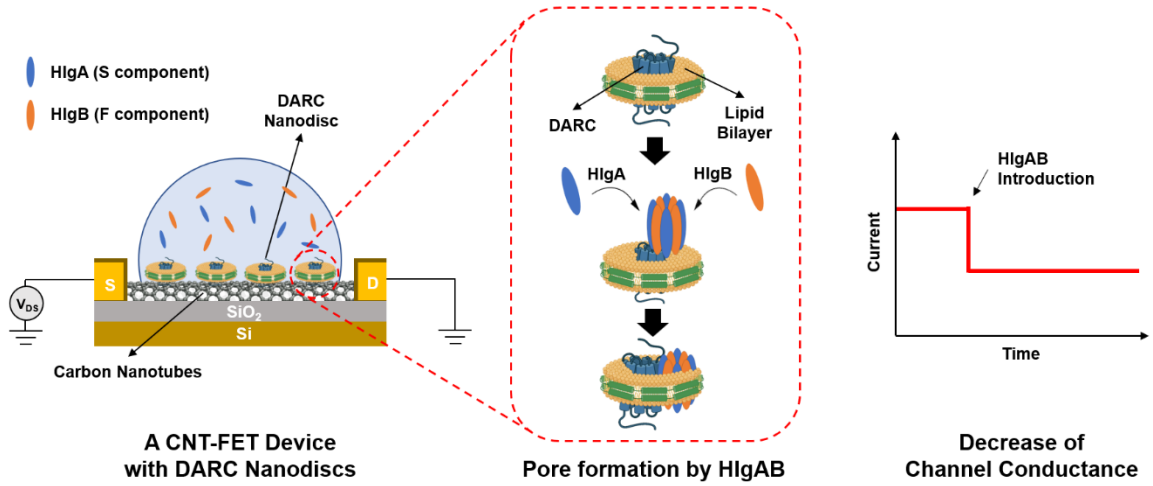
HlgA (S component)
HlgB (F component)
DARC Nanodisc
S
D
V_{DS}
SiO_2
Si
Carbon Nanotubes
A CNT-FET Device with DARC Nanodiscs
DARC
Lipid Bilayer
HlgA
HlgB
Pore formation by HlgAB
HlgAB Introduction
Current
Time
Decrease of Channel Conductance

Figure 2.

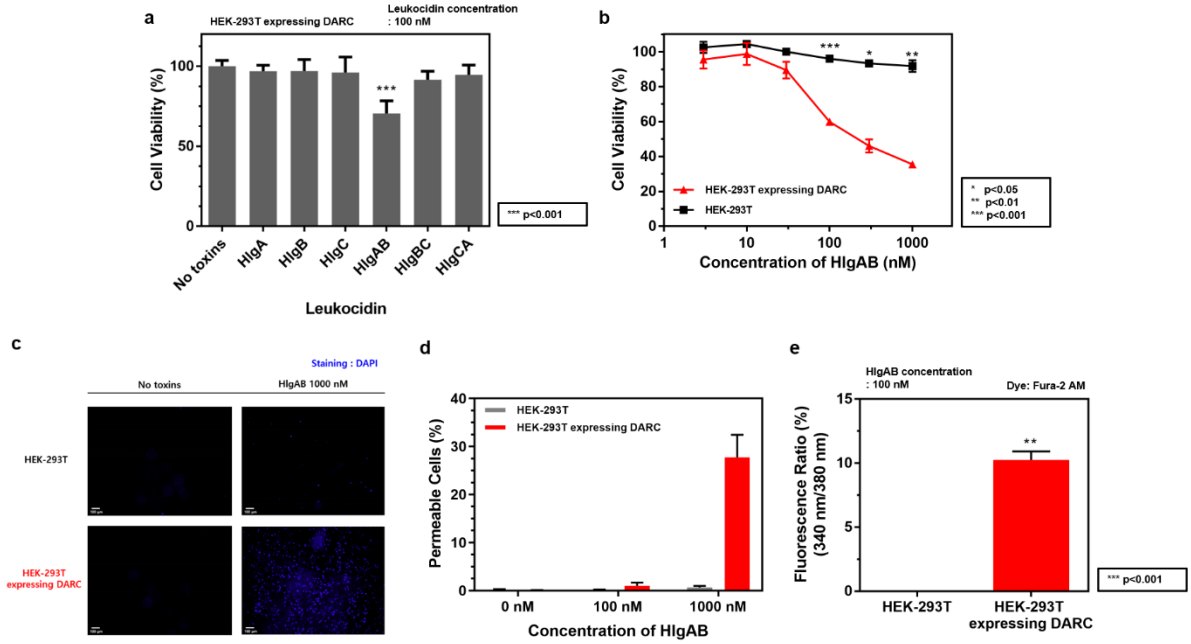
a
HEK-293T expressing DARC
Leukocidin concentration
: 100 nM
Cell Viability (%)
100
50
0
***
*** p<0.001
No toxins
HlgA
HlgB
HlgC
HlgAB
HlgBC
HlgCA
Leukocidin
b
Cell Viability (%)
100
80
60
40
20
0
***
*
**
HEK-293T expressing DARC
HEK-293T
* p<0.05
** p<0.01
*** p<0.001
1
10
100
1000
Concentration of HlgAB (nM)
c
Staining : DAPI
No toxins
HlgAB 1000 nM
HEK-293T
HEK-293T
expressing DARC
d
Permeable Cells (%)
40
30
20
10
0
HEK-293T
HEK-293T expressing DARC
0 nM
100 nM
1000 nM
Concentration of HlgAB
e
HlgAB concentration
: 100 nM
Dye: Fura-2 AM
Fluorescence Ratio (%)
(340 nm/380 nm)
15
10
5
0
**
*** p<0.001
HEK-293T
HEK-293T
expressing DARC

605 Figure 3.

606

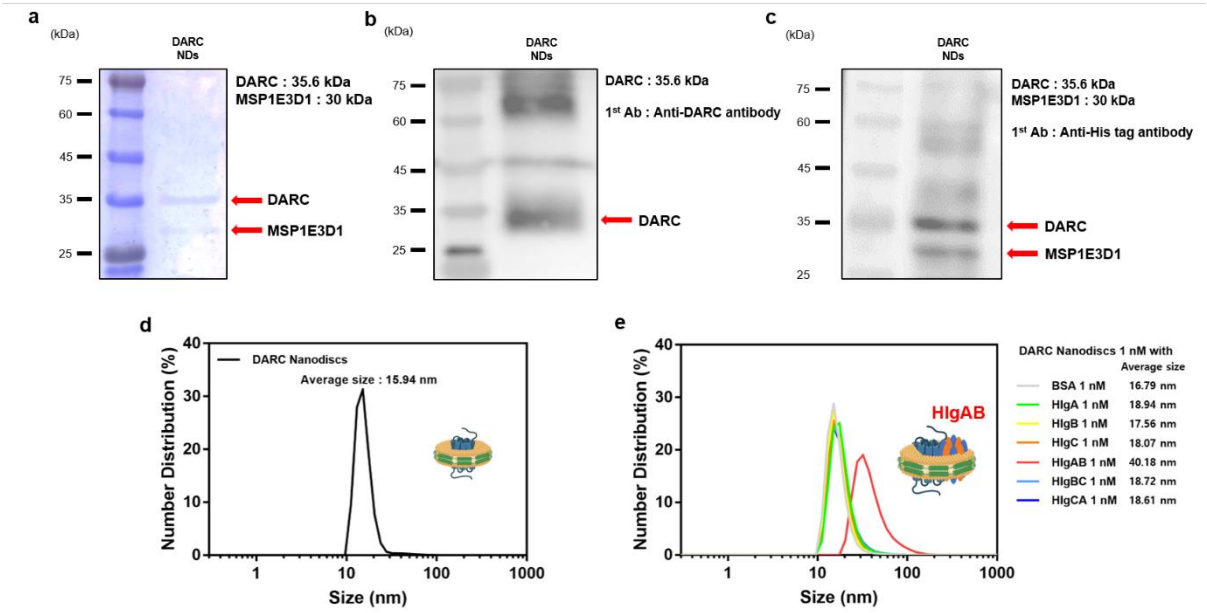

607

608

609 Figure 4.

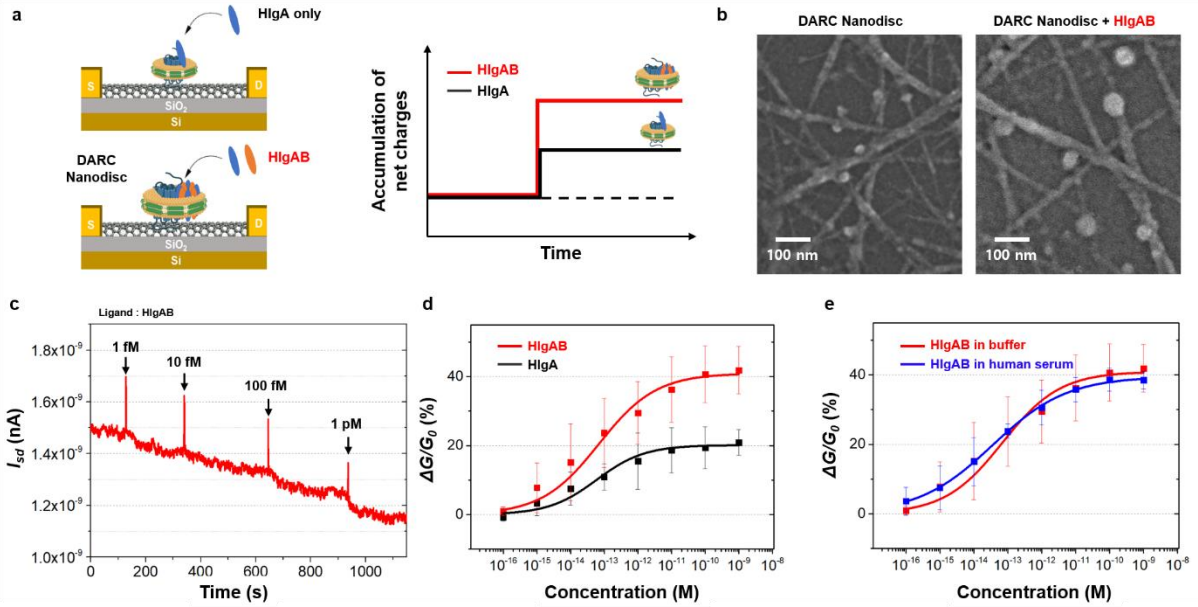

610

611

References

(1) Yamazaki, Y.; Ito, T.; Tamai, M.; Nakagawa, S.; Nakamura, Y. The role of Staphylococcus aureus quorum sensing in cutaneous and systemic infections. *Inflammation and Regeneration* **2024**, *44* (1), 9.

(2) Smith, H. Opportunistic infection. *British Medical Journal* **1973**, *2* (5858), 107.

(3) Thwaites, G. E.; Edgeworth, J. D.; Gkrania-Klotsas, E.; Kirby, A.; Tilley, R.; Török, M. E.; Walker, S.; Wertheim, H. F.; Wilson, P.; Llewelyn, M. J. Clinical management of Staphylococcus aureus bacteraemia. *The Lancet infectious diseases* **2011**, *11* (3), 208-222.

(4) Larsen, J.; Raisen, C. L.; Ba, X.; Sadgrove, N. J.; Padilla-González, G. F.; Simmonds, M. S.; Loncaric, I.; Kerschner, H.; Apfalter, P.; Hartl, R. Emergence of methicillin resistance predates the clinical use of antibiotics. *Nature* **2022**, *602* (7895), 135-141.

(5) Bagnoli, F.; Rappuoli, R.; Grandi, G. Staphylococcus aureus. *Cham: Springer International Publishing AG* **2017**.

(6) Van Hal, S. J.; Jensen, S. O.; Vaska, V. L.; Espedido, B. A.; Paterson, D. L.; Gosbell, I. B. Predictors of mortality in Staphylococcus aureus bacteremia. *Clinical microbiology reviews* **2012**, *25* (2), 362-386.

(7) Holland, T. L.; Arnold, C.; Fowler, V. G. Clinical management of Staphylococcus aureus bacteremia: a review. *Jama* **2014**, *312* (13), 1330-1341.

(8) Alonzo III, F.; Torres, V. J. The bicomponent pore-forming leucocidins of Staphylococcus aureus. *Microbiology and Molecular Biology Reviews* **2014**, *78* (2), 199-230.

(9) Skaar, E. P.; Humayun, M.; Bae, T.; DeBord, K. L.; Schneewind, O. Iron-source preference of Staphylococcus aureus infections. *Science* **2004**, *305* (5690), 1626-1628.

(10) Alfano, D. N.; Wardenburg, J. B. Another score for the pore: S. aureus leukocidins take a shot on the endothelium. *Cell Host & Microbe* **2019**, *25* (3), 351-353.

(11) Spaan, A. N.; Reyes-Robles, T.; Badiou, C.; Cochet, S.; Boguslawski, K. M.; Yoong, P.; Day, C. J.; de Haas, C. J.; van Kessel, K. P.; Vandenesch, F. Staphylococcus aureus targets the Duffy antigen receptor for chemokines (DARC) to lyse erythrocytes. *Cell host & microbe* **2015**, *18* (3), 363-370.

(12) Lubkin, A.; Lee, W. L.; Alonzo, F.; Wang, C.; Aligo, J.; Keller, M.; Girgis, N. M.; Reyes-Robles, T.; Chan, R.; O'Malley, A. Staphylococcus aureus leukocidins target endothelial DARC to cause lethality in mice. *Cell host & microbe* **2019**, *25* (3), 463-470. e469.

(13) Yoong, P.; Torres, V. J. The effects of Staphylococcus aureus leukotoxins on the host: cell lysis and beyond. *Current opinion in microbiology* **2013**, *16* (1), 63-69.

(14) Aman, M. J.; Adhikari, R. P. Staphylococcal bicomponent pore-forming toxins: targets for prophylaxis and immunotherapy. *Toxins* **2014**, *6* (3), 950-972.

(15) Yamashita, K.; Kawai, Y.; Tanaka, Y.; Hirano, N.; Kaneko, J.; Tomita, N.; Ohta, M.; Kamio, Y.; Yao, M.; Tanaka, I. Crystal structure of the octameric pore of staphylococcal γ-hemolysin reveals the β-barrel pore formation mechanism by two components. *Proceedings of the National Academy of Sciences*

2011, *108* (42), 17314-17319.
(16) Duan, R.; Wang, P. Rapid and Simple Approaches for Diagnosis of in Bloodstream Infections. *Polish Journal of Microbiology* **2022**, *71* (4), 481-489.
(17) Badiou, C.; Dumitrescu, O.; George, N.; Forbes, A. R.; Drougka, E.; Chan, K. S.; Ramdani-Bouguessa, N.; Meugnier, H.; Bes, M.; Vandenesch, F. Rapid detection of Staphylococcus aureus Panton-Valentine leukocidin in clinical specimens by enzyme-linked immunosorbent assay and immunochromatographic tests. *Journal of clinical microbiology* **2010**, *48* (4), 1384-1390.
(18) Reddy, P. K.; Shekar, A.; Kingston, J. J.; Sripathy, M. H.; Batra, H. Evaluation of IgY capture ELISA for sensitive detection of Alpha hemolysin of Staphylococcus aureus without staphylococcal protein A interference. *Journal of immunological methods* **2013**, *391* (1-2), 31-38.
(19) Lazcka, O.; Del Campo, F. J.; Munoz, F. X. Pathogen detection: A perspective of traditional methods and biosensors. *Biosensors and bioelectronics* **2007**, *22* (7), 1205-1217.
(20) Kang, C. D.; Lee, S. W.; Park, T. H.; Sim, S. J. Performance enhancement of real-time detection of protozoan parasite, Cryptosporidium oocyst by a modified surface plasmon resonance (SPR) biosensor. *Enzyme and microbial technology* **2006**, *39* (3), 387-390.
(21) Son, M.; Kim, D.; Kang, J.; Lim, J. H.; Lee, S. H.; Ko, H. J.; Hong, S.; Park, T. H. Bioelectronic nose using odorant binding protein-derived peptide and carbon nanotube field-effect transistor for the assessment of Salmonella contamination in food. *Analytical chemistry* **2016**, *88* (23), 11283-11287.
(22) Yang, H.; Kim, D.; Kim, J.; Moon, D.; Song, H. S.; Lee, M.; Hong, S.; Park, T. H. Nanodisc-based bioelectronic nose using olfactory receptor produced in Escherichia coli for the assessment of the death-associated odor cadaverine. *Acs Nano* **2017**, *11* (12), 11847-11855.
(23) Park, S. J.; Song, H. S.; Kwon, O. S.; Chung, J. H.; Lee, S. H.; An, J. H.; Ahn, S. R.; Lee, J. E.; Yoon, H.; Park, T. H. Human dopamine receptor nanovesicles for gate-potential modulators in high-performance field-effect transistor biosensors. *Scientific Reports* **2014**, *4* (1), 4342.
(24) Son, M.; Lee, J. Y.; Ko, H. J.; Park, T. H. Bioelectronic nose: An emerging tool for odor standardization. *Trends in biotechnology* **2017**, *35* (4), 301-307.
(25) Luo, Z.; Zhang, L.; Zeng, R.; Su, L.; Tang, D. Near-infrared light-excited core–core–shell UCNP@ Au@ CdS upconversion nanospheres for ultrasensitive photoelectrochemical enzyme immunoassay. *Analytical chemistry* **2018**, *90* (15), 9568-9575.
(26) Huang, L.; Chen, J.; Yu, Z.; Tang, D. Self-powered temperature sensor with seebeck effect transduction for photothermal–thermoelectric coupled immunoassay. *Analytical chemistry* **2020**, *92* (3), 2809-2814.
(27) Suaifan, G. A.; Alhogail, S.; Zourob, M. Rapid and low-cost biosensor for the detection of Staphylococcus aureus. *Biosensors and Bioelectronics* **2017**, *90*, 230-237.
(28) Rubab, M.; Shahbaz, H. M.; Olaimat, A. N.; Oh, D.-H. Biosensors for rapid and sensitive detection of Staphylococcus aureus in food. *Biosensors and Bioelectronics* **2018**, *105*, 49-57.
(29) Gong, H.; Chen, F.; Huang, Z.; Gu, Y.; Zhang, Q.; Chen, Y.; Zhang, Y.; Zhuang, J.; Cho, Y.-K.; Fang,

R. H. Biomembrane-modified field effect transistors for sensitive and quantitative detection of biological toxins and pathogens. *ACS nano* **2019**, *13* (3), 3714-3722.
(30) Kim, I.; Kim, Y.; Lee, S. W.; Lee, D.; Jung, H. G.; Jang, J. W.; Lee, T.; Yoon, Y. K.; Lee, G.; Yoon, D. S. Erythrocyte-camouflaged biosensor for α-hemolysin detection. *Biosensors and Bioelectronics* **2021**, *185*, 113267.
(31) Andersson, T.; Bläckberg, A.; Lood, R.; Ertürk Bergdahl, G. Development of a molecular imprinting-based surface plasmon resonance biosensor for rapid and sensitive detection of Staphylococcus aureus alpha hemolysin from human serum. *Frontiers in cellular and infection microbiology* **2020**, *10*, 571578.
(32) Michalke, K.; Gravière, M.-E.; Huyghe, C.; Vincentelli, R.; Wagner, R.; Pattus, F.; Schroeder, K.; Oschmann, J.; Rudolph, R.; Cambillau, C. Mammalian G-protein-coupled receptor expression in Escherichia coli: I. High-throughput large-scale production as inclusion bodies. *Analytical biochemistry* **2009**, *386* (2), 147-155.
(33) Song, H. S.; Lee, S. H.; Oh, E. H.; Park, T. H. Expression, solubilization and purification of a human olfactory receptor from Escherichia coli. *Current microbiology* **2009**, *59*, 309-314.
(34) Goldsmith, B. R.; Mitala Jr, J. J.; Josue, J.; Castro, A.; Lerner, M. B.; Bayburt, T. H.; Khamis, S. M.; Jones, R. A.; Brand, J. G.; Sligar, S. G. Biomimetic chemical sensors using nanoelectronic readout of olfactory receptor proteins. *ACS nano* **2011**, *5* (7), 5408-5416.
(35) Oh, J.; Yang, H.; Jeong, G. E.; Moon, D.; Kwon, O. S.; Phyo, S.; Lee, J.; Song, H. S.; Park, T. H.; Jang, J. Ultrasensitive, selective, and highly stable bioelectronic nose that detects the liquid and gaseous cadaverine. *Analytical chemistry* **2019**, *91* (19), 12181-12190.
(36) Denisov, I. G.; Sligar, S. G. Nanodiscs in membrane biochemistry and biophysics. *Chemical reviews* **2017**, *117* (6), 4669-4713.
(37) Denisov, I. G.; Sligar, S. G. Nanodiscs for structural and functional studies of membrane proteins. *Nature structural & molecular biology* **2016**, *23* (6), 481-486.
(38) Seilie, E. S.; Wardenburg, J. B. Staphylococcus aureus pore-forming toxins: The interface of pathogen and host complexity. In *Seminars in cell & developmental biology*, 2017; Elsevier: Vol. 72, pp 101-116.
(39) Spaan, A. N.; van Strijp, J. A.; Torres, V. J. Leukocidins: staphylococcal bi-component pore-forming toxins find their receptors. *Nature Reviews Microbiology* **2017**, *15* (7), 435-447.
(40) Mishra, S.; Roy, A.; Dutta, S. Cryo-EM-based structural insights into supramolecular assemblies of γ-hemolysin from S. aureus reveal the pore formation mechanism. *Structure* **2023**, *31* (6), 651-667. e655.
(41) Gasteiger, E.; Hoogland, C.; Gattiker, A.; Duvaud, S. e.; Wilkins, M. R.; Appel, R. D.; Bairoch, A. *Protein identification and analysis tools on the ExPASy server*; Springer, 2005.
(42) Josuran, R. *Prot pi*. 2014. www.protpi.ch (accessed April 1, 2024.)
(43) Hanlon, A. D.; Larkin, M. I.; Reddick, R. M. Free-solution, label-free protein-protein interactions

722 characterized by dynamic light scattering. *Biophysical journal* **2010**, *98* (2), 297-304.
723 (44) Stetefeld, J.; McKenna, S. A.; Patel, T. R. Dynamic light scattering: a practical guide and
724 applications in biomedical sciences. *Biophysical reviews* **2016**, *8*, 409-427.
725 (45) Vasquez, M. T.; Lubkin, A.; Reyes-Robles, T.; Day, C. J.; Lacey, K. A.; Jennings, M. P.; Torres, V. J.
726 Identification of a domain critical for Staphylococcus aureus LukED receptor targeting and lysis of
727 erythrocytes. *Journal of Biological Chemistry* **2020**, *295* (50), 17241-17250.
728 (46) Padmanabha Das, K. M.; Shih, W. M.; Wagner, G.; Nasr, M. L. Large nanodiscs: a potential game
729 changer in structural biology of membrane protein complexes and virus entry. *Frontiers in*
730 *Bioengineering and Biotechnology* **2020**, *8*, 539.
731 (47) Gao, Y.; Yu, Z.; Huang, L.; Zeng, Y.; Liu, X.; Tang, D. Photoinduced electron transfer modulated
732 photoelectric signal: toward an organic small molecule-based photoelectrochemical platform for
733 formaldehyde detection. *Analytical chemistry* **2023**, *95* (23), 9130-9137.
734 (48) Bhardwaj, S. K.; Chauhan, R.; Yadav, P.; Ghosh, S.; Mahapatro, A. K.; Singh, J.; Basu, T. Bi-enzyme
735 functionalized electro-chemically reduced transparent graphene oxide platform for triglyceride
736 detection. *Biomaterials science* **2019**, *7* (4), 1598-1606.
737 (49) Macchia, E.; De Caro, L.; Torricelli, F.; Franco, C. D.; Mangiatordi, G. F.; Scamarcio, G.; Torsi, L. Why
738 a Diffusing Single-Molecule can be Detected in Few Minutes by a Large Capturing Bioelectronic
739 Interface. *Advanced Science* **2022**, *9* (20), 2104381.
740 (50) Lagerholm, B. C.; Thompson, N. L. Theory for ligand rebinding at cell membrane surfaces.
741 *Biophysical journal* **1998**, *74* (3), 1215-1228.
742 (51) Ferreras, M.; Höper, F.; Dalla Serra, M.; Colin, D. A.; Prévost, G.; Menestrina, G. The interaction of
743 Staphylococcus aureus bi-component γ-hemolysins and leucocidins with cells and lipid membranes.
744 *Biochimica et Biophysica Acta (BBA)-Biomembranes* **1998**, *1414* (1-2), 108-126.
745 (52) Potrich, C.; Bastiani, H.; Colin, D.; Huck, S.; Prevost, G.; Dalla Serra, M. The influence of membrane
746 lipids in Staphylococcus aureus gamma-hemolysins pore formation. *Journal of Membrane Biology*
747 **2009**, *227*, 13-24.
748 (53) Ba, V. A. P.; Cho, D.-g.; Kim, D.; Yoo, H.; Ta, V.-T.; Hong, S. Quantitative electrophysiological
749 monitoring of anti–histamine drug effects on live cells via reusable sensor platforms. *Biosensors and*
750 *Bioelectronics* **2017**, *94*, 707-713.
751 (54) Park, I.; Yang, I.; Cho, Y.; Choi, Y.; Shin, J.; Shekhar, S.; Lee, S. H.; Hong, S. Evaluation of site-
752 selective drug effects on GABA receptors using nanovesicle-carbon nanotube hybrid devices.
753 *Biosensors and Bioelectronics* **2022**, *200*, 113903.
754 (55) Kwiecinski, J. M.; Horswill, A. R. Staphylococcus aureus bloodstream infections: pathogenesis
755 and regulatory mechanisms. *Current opinion in microbiology* **2020**, *53*, 51-60.
756 (56) Malachowa, N.; Whitney, A. R.; Kobayashi, S. D.; Sturdevant, D. E.; Kennedy, A. D.; Braughton, K.
757 R.; Shabb, D. W.; Diep, B. A.; Chambers, H. F.; Otto, M. Global changes in Staphylococcus aureus
758 gene expression in human blood. *PloS one* **2011**, *6* (4), e18617.

(57) *ATCC Genome Portal*. https://genomes.atcc.org/genomes/79f43b45f79b4abc (accessed April 1, 2024.)

(58) Suo, B.; Yang, H.; Wang, Y.; Lv, H.; Li, Z.; Xu, C.; Ai, Z. Comparative proteomic and morphological change analyses of Staphylococcus aureus during resuscitation from prolonged freezing. *Frontiers in Microbiology* **2018**, *9*, 866.

(59) Pivard, M.; Caldelari, I.; Brun, V.; Croisier, D.; Jaquinod, M.; Anzala, N.; Gilquin, B.; Teixeira, C.; Benito, Y.; Couzon, F. Complex Regulation of Gamma-Hemolysin Expression Impacts Staphylococcus aureus Virulence. *Microbiology Spectrum* **2023**, *11* (4), e01073-01023.

(60) Stulik, L.; Rouha, H.; Labrousse, D.; Visram, Z. C.; Badarau, A.; Maierhofer, B.; Groß, K.; Weber, S.; Kramarić, M. D.; Glojnarić, I. Preventing lung pathology and mortality in rabbit Staphylococcus aureus pneumonia models with cytotoxin-neutralizing monoclonal IgGs penetrating the epithelial lining fluid. *Scientific Reports* **2019**, *9* (1), 5339.

(61) Sessi, V.; Ibarlucea, B.; Seichepine, F.; Klinghammer, S.; Ibrahim, I.; Heinzig, A.; Szabo, N.; Mikolajick, T.; Hierlemann, A.; Frey, U. Multisite dopamine sensing with femtomolar resolution using a CMOS enabled aptasensor chip. *Frontiers in neuroscience* **2022**, *16*, 875656.

(62) Monecke, S.; Müller, E.; Buechler, J.; Rejman, J.; Stieber, B.; Akpaka, P. E.; Bandt, D.; Burris, R.; Coombs, G.; Hidalgo-Arroyo, G. A. Rapid detection of Panton-Valentine leukocidin in Staphylococcus aureus cultures by use of a lateral flow assay based on monoclonal antibodies. *Journal of Clinical Microbiology* **2013**, *51* (2), 487-495.

For TOC only

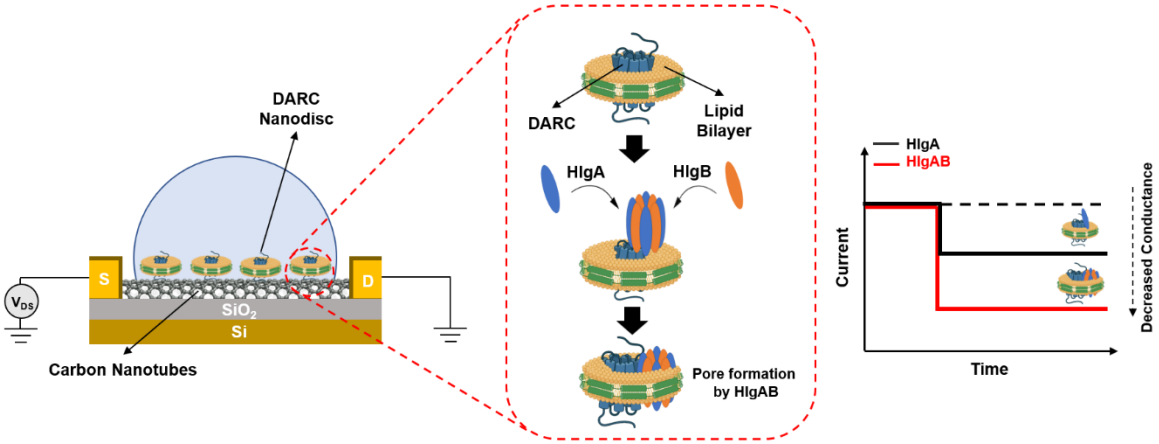
DARC
Nanodisc
S
D
V_{DS}
SiO_2
Si
Carbon Nanotubes
DARC
Lipid
Bilayer
HlgA
HlgB
Pore formation
by HlgAB
HlgA
HlgAB
Current
Time
Decreased Conductance